Effect of nitrogen doping and pressure on the stability of cubic LuH_3

Yang Sun,[1,2] Feng Zhang,[2] Shunqing Wu,[1] Vladimir Antropov,[2] and Kai-Ming Ho[2]

[1] *Department of Physics, Xiamen University, Xiamen 361005, China*

[2] *Department of Physics, Iowa State University, Ames, IA 50011, USA*

(Dated: Mar. 24, 2023)

The report on the near-ambient superconductivity in a nitrogen-doped lutetium hydride has stimulated great interest in this material (Dasenbrock-Gammon et al. 2023). While its superconductivity is still a subject of debate, the structure of the claimed cubic phase remains uncertain. In this work, we study the effect of nitrogen doping and pressure on the energetic and dynamic stability of cubic LuH_3. Our findings indicate that both pressure and nitrogen doping can enhance the stability of the cubic LuH_3 phase. We propose a $Lu_8H_{21}N$ structure that exhibits stable phonon, reasonable thermodynamics stability at 1 GPa, and a similar XRD pattern to the experimental data. However, we do not observe electron-phonon coupling in the zone-center phonon modes of these crystal structures.

I. INTRODUCTION

The search for room-temperature superconductors under ambient conditions is a huge scientific challenge that can lead to many applications. More than 50 years ago Ashcroft and Ginzburg already discussed the possibility of having such superconductivity in the metallic phase of hydrogen [1, 2]. Only recently, it became possible to predict and observe new hydrogen-rich metallic phases with such superconductivity [3].

High-pressure experiments have had great success in discovering many high-T_c hydrides, such as H_3S with T_c above 200 K under 200 GPa [4], LaH_{10} with $T_c \sim$ 250K at 170GPa [5, 6], ThH_{10} with $T_c \sim$ 160K at ∼170GPa [7], CeH_{10} with $T_c \sim$ 115K at 95GPa [8], YH_6 with $T_c \sim$ 224K at ∼166GPa [9, 10], YH_9 with $T_c \sim$ 262K at ∼180GPa [10, 11], CaH_6 with $T_c \sim$ 215K at 172GPa [12]. However, such high pressures are still too extreme for practical applications. Therefore, doping or substituting hydrogen with other light elements such as B, C, and N has been proposed to lower the required high pressure [13–22].

Recently, Dasenbrock-Gammon et al. reported experimental evidence of superconductivity in N-doped Lutetium hydride near ambient conditions [23]. The material was synthesized at 2 GPa and claimed to achieve the T_c of 274 K at 1 GPa. However, the superconducting behavior of this phase is being questioned [24, 25], and the crystal structure of the synthesized phase is unclear. Dasenbrock-Gammon et al. described the structure as a cubic $LuH_{3-\delta}N_\epsilon$, where δ and ϵ are unknown values that account for the hydrogen vacancy defect and nitrogen contents, respectively. As the X-ray diffraction pattern is not sensitive to hydrogen and nitrogen, only the lattice parameter for the Lu sublattice was solved, as a cubic structure with a=5.0289(4) Å. Elemental analysis revealed a weight percent of 0.8-0.9% N in the materials. However, the cubic LuH_3 is known to be unstable under ambient conditions. Therefore, the unknown crystal structure makes the study of superconductivity in this compound difficult. In this work, we use the first-principle calculation to investigate the effects of pressure and N doping on the thermodynamic and dynamical stability of cubic LuH_3. Our aim is to find a stable structure model that can explain the experimental data reported in Dasenbrock-Gammon et al.

II. METHODS

Density functional theory (DFT) calculations were carried out using the projector augmented wave (PAW) method [26] implemented in the VASP code [27, 28]. PAW potentials with valence electronic configurations $6s^25d^15p^6$, $1s^1$, and $2s^22p^3$ were used for Lu, H, and N atoms, respectively. The exchange and correlation energy was treated with the generalized gradient approximation (GGA) and parameterized by the Perdew-Burke-Ernzerhof formula (PBE) [29]. A plane-wave basis was used with a kinetic energy cutoff of 520 eV, and the convergence criterion for the total energy was set to 10^{-8} eV. The Γ-centered Monkhorst-Pack grid was adopted for Brillouin zone sampling with a spacing of $2\pi \times 0.025$ Å^{-1}. The full Brillouin zone phonon spectrums were computed by the finite displacement method implemented in the Phonopy code [30] using $3 \times 3 \times 3$ supercell for LuH_3 (108 atoms) and $2 \times 2 \times 2$ supercell for $Lu_8H_{21}N$ (240 atoms). The zone-center electron-phonon coupling strength was calculated by the frozen-phonon method developed in [31].

III. RESULTS

A. Lu-H-N phase diagram

The binary LuN [32], LuH_2 [33] and LuH_3 [34] phases have been synthesized and documented in the experimental ICSD database, but no stable ternary Lu-H-N phase has been reported yet. Computational databases, such as Material Project [35] and OQMD [36], yield consistent results. As shown in Fig. 1, the Lu-H-N phase diagram at 1 GPa is relatively simple that only LuN, LuH_2, and LuH_3 are stable phases. Both LuN and LuH_2 have $Fm\bar{3}m$ structures, with Lu occupying the fcc sublattice. In LuN, N occupies the octahedral site, while in LuH_2, H occupies the tetrahedral site. The stable LuH_3 phase exhibits a rhombohedral structure (noted as r-LuH_3) with space group $P\bar{3}c1$, where Lu atoms pack in an hcp sublattice. The cubic LuH_3 (noted as c-LuH_3) shows a relatively high enthalpy, 85 meV/atom higher than r-LuH_3 at 1 GPa (Table I).

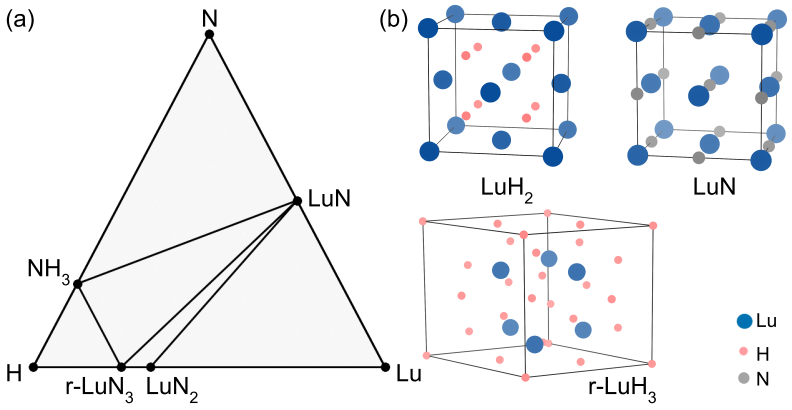

FIG. 1. The phase diagram of Lu-N-H system. (b) The crystal structure of LuH_2, LuN, and rhombohedral LuH_3.

TABLE I. Enthalpy above the convex hull of LuNH phases at 1GPa.

System	ΔH_{hull} (meV/atom)
LuH_2	0
Rhombohedral LuH_3	0
Cubic LuH_3	85
$Lu_4H_{11}N$, N at octahedral site	278
$Lu_4H_{11}N$, N at tetrahedral site	134
$Lu_8H_{23}N$, N at octahedral site	150
$Lu_8H_{23}N$, N at tetrahedral site	130
$Lu_8H_{21}N$, N at tetrahedral site	31

B. Pressure effect on cubic LuH_3

We first investigate the pressure effect on the stability of c-LuH_3. The phonon spectrums of c-LuH_3 at various pressures are shown in Fig. 2. At pressures of 1-5 GPa, the phonon modes show strong instability. As the pressure increases to ∼20 GPa, the imaginary phonon modes are significantly reduced. At 25GPa, c-LuH_3 does not show any imaginary phonon modes. The phonon density of states shows that the H atoms at the tetrahedral site have much higher frequencies than those at octahedral sites. At 25 GPa, the enthalpy of c-LuH_3 is only 12 meV/atom higher than that of r-LuH_3, which is significantly reduced compared to 85 meV/atom at 1 GPa. These results suggest that high-pressure conditions can stabilize c-LuH_3 both energetically and mechanically.

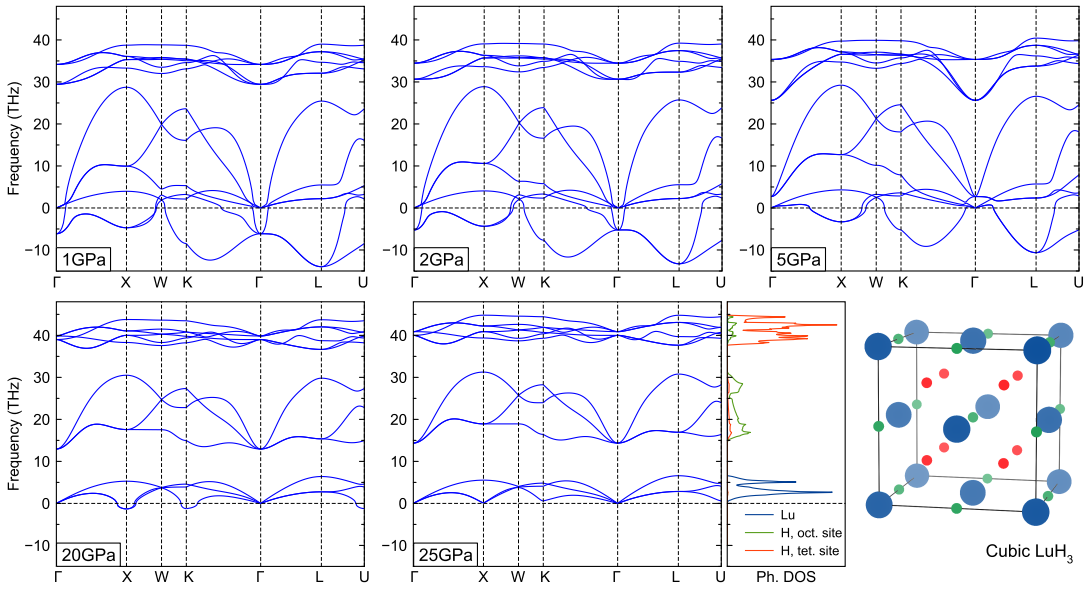

FIG. 2. The phonon spectrum for cubic LuH_3 as a function of pressures. The imaginary modes disappear when the pressure is higher than ∼25 GPa. The phonon density of states (Ph. DOS) is shown for the data at 25 GPa. In the atomic structure of cubic LuH_3, red shows H at the tetrahedral sites, while green shows H at the octahedral sites. Blue is Lu atoms.

C. N doping effect on cubic LuH_3

Although pressure can stabilize LuH_3, the condition of 25 GPa is too high compared to the near-ambient condition reported in Dasenbrock-Gammon et al. [23]. Hence, we dope the N in the c-LuH_3 to study its effect on the stability at 1 GPa. We first use a conventional c-LuH_3 cell (4 f.u.) and substitute the H at octahedral and tetrahedral sites, respectively, resulting in $Lu_4H_{11}N$. At 1 GPa, the enthalpies of both phases above the convex hull are largely positive (Table I), even higher than c-LuH_3. The enthalpy of N at tetrahedral sites is lower than that at the octahedral site, indicating N's preference for the tetrahedral sites of c-LuH_3. Doping N at the octahedral site did not significantly alter the structure. However, doping at the tetrahedral site causes a change in the local H positions. As shown in Fig. 3(a), N repels the surrounding H atoms, leading to the formation of short H-H bonds and a local H tetrahedron. The N content in $Lu_4H_{11}N$ is 1.9 wt.%, which is twice larger than the ones (0.8-0.9 wt.%) reported in Dasenbrock-Gammon et al. [23]. To be closer to experimental condition, we use a $\sqrt{2} \times \sqrt{2} \times 1$ supercell (8 f.u.) and replace one H with N to reduce the doping concentration, yielding $Lu_8H_{23}N$. As shown in Table. 1, $Lu_8H_{23}N$ with N at the tetrahedral site still shows a lower enthalpy than that at the octahedral site. Thus, if N is doped into the c-LuH_3, it is expected to occupy the tetrahedral sites. Both $Lu_4H_{11}N$ and $Lu_8H_{23}N$ show strong imaginary phonons in Fig. 3 and higher relative enthalpy above the convex hull compared to c-LuH_3. Therefore, these phases are still unstable and cannot be used to model the experimentally claimed $LuH_{3-\delta}N_\epsilon$ phase [23].

By analyzing the phonon instability at the zone center in $Lu_8H_{23}N$, we find it's mainly caused by H atoms with shortened H bonds. To eliminate these instabilities, we introduce vacancies at the H sites that are closely related to these short bonds (circled sites in Fig. 3b). This generates a model with stoichiometry $Lu_8H_{21}N$. After relaxing this model, we find the phonon instability disappears, as shown in Fig. 4. Moreover, by introducing the defects, the enthalpy above the convex hull decreases to 31 meV/atom (Table I). Thus, these defects significantly improve both thermodynamic and dynamic stability. As this structure contains 14 tetrahedral sites with 2 vacancies, the N atom can also replace other tetrahedral sites equivalently. It could form solid solutions at finite temperatures, introducing configurational entropy to further lower the free energy. If we estimate the configurational entropy with the ideal solid solution model, the free energy above the convex hull is ∼24 meV/atom at 294 K, which is within the room temperature fluctuation. Therefore, from the perspective of energetics and dynamical stabilities, this $Lu_8H_{21}N$ structure can exist under near-ambient conditions.

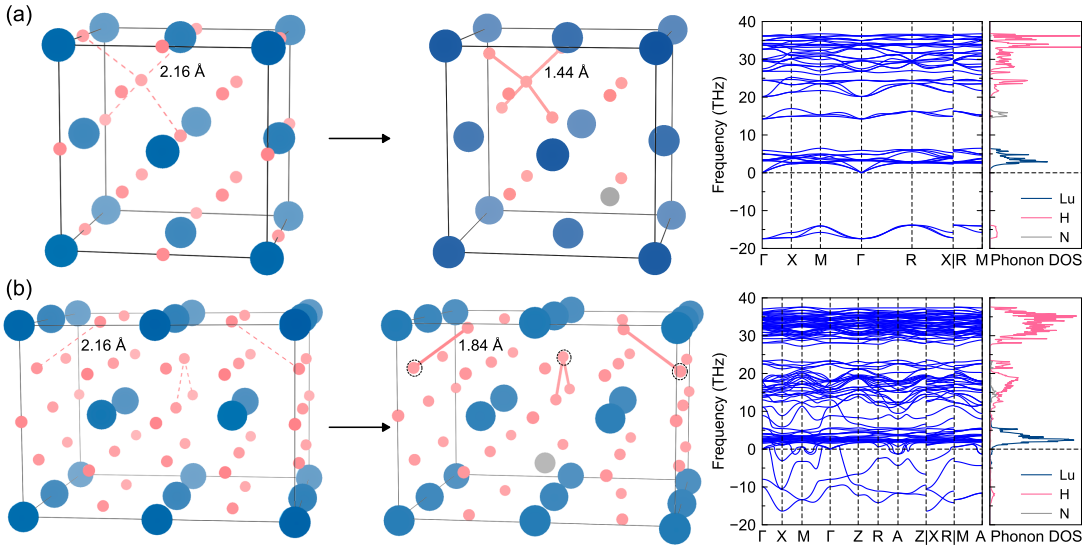

FIG. 3. The structural change in (a) $Lu_4H_{11}N$ and (b) $Lu_8H_{23}N$ due to the N doping at the tetrahedral site at 1 GPa. The connected H-H bonds are the shortened bonds caused by the N substitution. The right panels show the phonon spectrum and phonon density of states of doped structures.

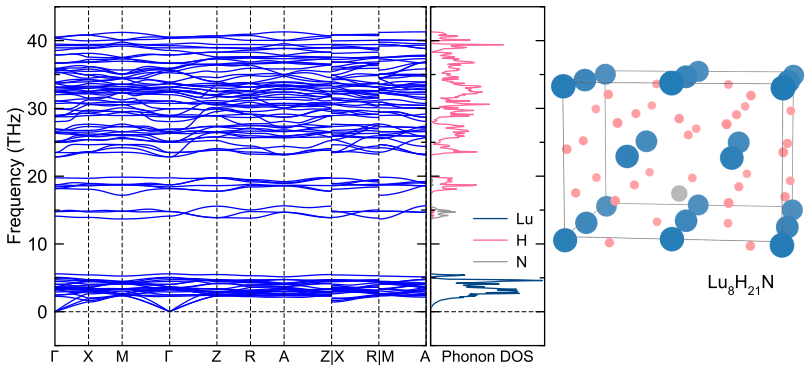

FIG. 4. The phonon spectrum and atomic structure of $Lu_8H_{21}N$ at 1 GPa.

D. Comparison of XRD patterns

We compare the XRD of $Lu_8H_{21}N$ structures with the experimental data reported in Ref. [23]. The peak of $Lu_8H_{21}N$ XRD shows good agreement with experimental XRD without any refinement, although some small differences exist. Firstly, it shows small peak splitting at $2\theta = 35°, 51°$ and $61°$. These splitting are relatively small, even less than the FWHM of corresponding experimental peaks. They are mainly due to the change of lattice symmetry. With full DFT relaxation, the stoichiometric $Lu_8H_{21}N$ model is a tetragonal phase with space group $P\bar{4}m2$ (see crystallographic data in Supplementary Material Table S1). The a/c ratio is 1.382, which deviates from the original $\sqrt{2}$ ratio in the supercell of the cubic lattice. However, if it forms a solid solution at a finite temperature and N is randomly distributed to the tetrahedral sites, the phase should recover the cubic lattice. Secondly, there is a systematical shift of the peak positions of the fully relaxed structure compared to the experimental data. This is due to the lattice parameter difference. The experimental XRD can be solved by the cubic lattice with a=5.0289 Å, while the fully relaxed cell has c=5.1951 Å. This may be attributed to the PBE functional that constantly overestimates the cell volume compared to the experimental measurement. To eliminate the effect of these two factors, we change the $Lu_8H_{21}N$ lattice to experimental one a=b=5.0289 $\times \sqrt{2}$ Å and c=5.0289 Å, while keeping atom positions fixed. This leads to an XRD that matches all the main peaks of the experimental data.

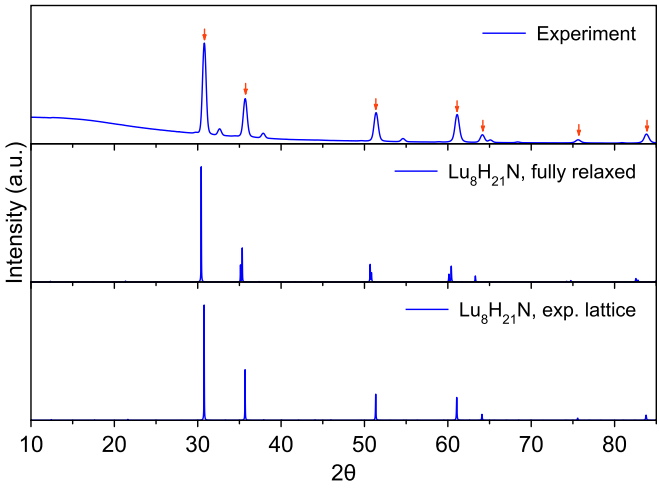

FIG. 5. Comparison of XRD between experimental data from [23] and $Lu_8H_{21}N$ model with different lattices. Red arrows indicate the indexed peaks. The remaining peak can be explained by LuN+Lu_2O_3 as described in [23].

E. Zone-center electron-phonon coupling strength

We have demonstrated that both high pressure and N doping can stabilize the c-LuH_3 phase. To examine the possibility of superconductivity in this phase, we employ a recently developed frozen phonon method to compute the zone-center electron-phonon coupling (EPC) strength in the present structures. This efficient method can identify the strong EPC candidates in many hydrides because the zone-center EPC shows a strong correlation with the full Brillouin zone EPC in these materials [31]. In Fig. 6, we compute the screened (ω) and unscreened ($\tilde{\omega}$) zone-center phonon frequencies for LuH_3 at 1GPa and 25 GPa, as well as $Lu_8H_{21}N$ at 1 GPa, respectively. The zone-center EPC strength (λ_Γ) can be computed by the relative difference between two frequencies [31] as

$$\lambda_\Gamma = \frac{\tilde{\omega}^2 - \omega^2}{4\omega^2}. \tag{1}$$

We find the screened and unscreened phonon frequencies are almost the same, resulting in $\lambda_\Gamma \sim 0$ for all these materials. Therefore, the c-LuH_3 phase, regardless of whether it is compressed or N-doped, does not show strong EPC in the zone center.

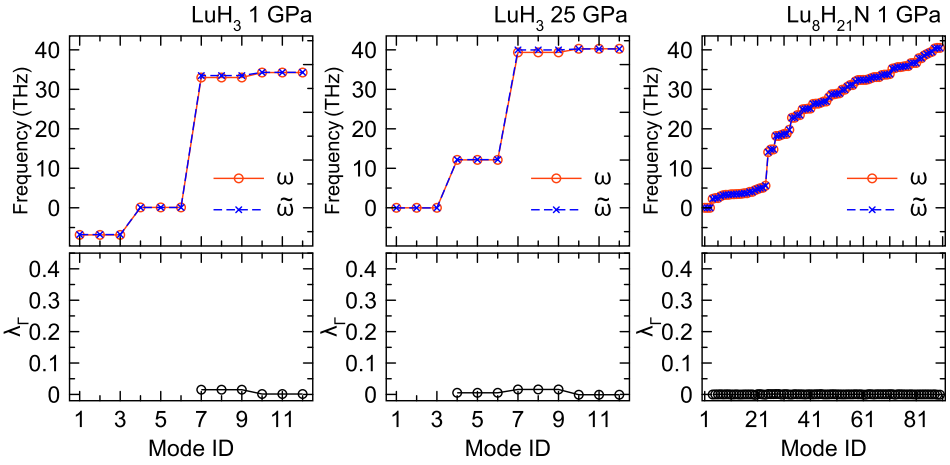

FIG. 6. Zone-center EPC strength. Upper panels show the screened and unscreened phonon frequencies and lower panels show the zone-center EPC strength.

IV. SUMMARY

In summary, we show that both pressure and nitrogen doping can improve the thermodynamic and structural stability of cubic LuH_3. A pressure of 25 GPa can stabilize the phonon spectrum of the cubic LuH_3 and reduce its enthalpy difference with respect to the stable rhombohedral LuH_3 to 12 meV/atom. However, this condition is too far from the recently reported experimental condition in Dasenbrock-Gammon et al. We find that a more realistic way to stabilize the cubic LuH_3 is to substitute hydrogen atoms at the tetrahedral sites with nitrogen atoms and introduce vacancies to release the local distortion of hydrogen atoms. This can simultaneously stabilize the phonon spectrum and improve thermodynamic stability. We propose the $Lu_8H_{21}N$ model to address the experimentally synthesized material. In addition, by examining the zone-center electron-phonon coupling, we cannot find any theoretical evidence of strong superconductivity in these structures.

[1] N. W. Ashcroft, Metallic Hydrogen: A High-Temperature Superconductor?, Phys Rev Lett 21, 1748 (1968).
[2] V. L. Ginzburg, Superfluidity and Superconductivity in the Universe, Soviet Physics Uspekhi 12, 241 (1969).
[3] L. Boeri et al., The 2021 Room-Temperature Superconductivity Roadmap, J Phys Condens Matter 34, 183002 (2022).
[4] A. P. Drozdov, M. I. Eremets, I. A. Troyan, V. Ksenofontov, and S. I. Shylin, Conventional Superconductivity at 203 Kelvin at High Pressures in the Sulfur Hydride System, Nature 525, 73 (2015).
[5] M. Somayazulu, M. Ahart, A. K. Mishra, Z. M. Geballe, M. Baldini, Y. Meng, V. V. Struzhkin, and R. J. Hemley, Evidence for Superconductivity above 260 K in Lanthanum Superhydride at Megabar Pressures, Phys Rev Lett 122, 027001 (2019).
[6] A. P. Drozdov et al., Superconductivity at 250 K in Lanthanum Hydride under High Pressures, Nature 569, 528 (2019).
[7] D. V. Semenok, A. G. Kvashnin, A. G. Ivanova, V. Svitlyk, V. Y. Fominski, A. V. Sadakov, O. A. Sobolevskiy, V. M. Pudalov, I. A. Troyan, and A. R. Oganov, Superconductivity at 161 K in Thorium Hydride ThH_{10}: Synthesis and Properties, Materials Today 33, 36 (2020).
[8] W. Chen, D. V. Semenok, X. Huang, H. Shu, X. Li, D. Duan, T. Cui, and A. R. Oganov, High-Temperature Superconducting Phases in Cerium Superhydride with a T_c up to 115 K below a Pressure of 1 Megabar, Phys Rev Lett 127, 117001 (2021).
[9] I. A. Troyan et al., Anomalous High-Temperature Superconductivity in YH_6, Adv Mater 33, 2006832 (2021).
[10] P. Kong et al., Superconductivity up to 243 K in the Yttrium-Hydrogen System under High Pressure, Nat Comm 12, 5075 (2021).
[11] E. Snider, N. Dasenbrock-Gammon, R. McBride, X. Wang, N. Meyers, K. V. Lawler, E. Zurek, A. Salamat, and R. P. Dias, Synthesis of Yttrium Superhydride Superconductor with a Transition Temperature up to 262 K by Catalytic Hydrogenation at High Pressures, Phys Rev Lett 126, 117003 (2021).
[12] L. Ma et al., High-Temperature Superconducting Phase in Clathrate Calcium Hydride CaH_6 up to 215 K at a Pressure of 172 GPa, Phys Rev Lett 128, 167001 (2022).
[13] Y. Hou, B. Li, Y. Bai, X. Hao, Y. Yang, F. Chi, S. Liu, J. Cheng, and Z. Shi, Superconductivity in $CeBeH_8$ and $CeBH_8$ at Moderate Pressures, J Phys Condens Matter 34, 505403 (2022).
[14] T. T. Gai, P. J. Guo, H. C. Yang, Y. Gao, M. Gao, and Z. Y. Lu, Van Hove Singularity Induced Phonon-Mediated Superconductivity above 77 K in Hole-Doped SrB_3C_3, Phys Rev B 105, 224514 (2022).
[15] X. Li, X. Zhang, A. Bergara, Y. Liu, and G. Yang, Structural and Electronic Properties of Na-B-H Compounds at High Pressure, Phys Rev B 106, 174104 (2022).
[16] H. B. Ding, Y. J. Feng, M. J. Jiang, H. L. Tian, G. H. Zhong, C. L. Yang, X. J. Chen, and H. Q. Lin, Ambient-Pressure High-T_c Superconductivity in Doped Boron-Nitrogen Clathrates $La(BN)_5$ and $Y(BN)_5$, Phys Rev B 106, 104508 (2022).
[17] Z. Zhang, T. Cui, M. J. Hutcheon, A. M. Shipley, H. Song, M. Du, V. Z. Kresin, D. Duan, C. J. Pickard, and Y. Yao, Design Principles for High-Temperature Superconductors with a Hydrogen-Based Alloy Backbone at Moderate Pressure, Phys Rev Lett 128, 047001 (2022).
[18] N. Geng, T. Bi, and E. Zurek, Structural Diversity and Superconductivity in S–P–H Ternary Hydrides under Pressure, J Phys Chem C 126, 7208 (2022).
[19] S. Di Cataldo, W. Von Der Linden, and L. Boeri, Phase Diagram and Superconductivity of Calcium Borohyrides at Extreme Pressures, Phys Rev B 102, 014516 (2020).
[20] S. Di Cataldo, W. von der Linden, and L. Boeri, First-Principles Search of Hot Superconductivity in La-X-H Ternary Hydrides, npj Comput Mater 8, 2 (2022).
[21] F. Zheng, Y. Sun, R. Wang, Y. Fang, F. Zhang, S. Wu, C.-Z. Wang, V. Antropov, and K.-M. Ho, Superconductivity in the Li-B-C System at 100 GPa, Phys Rev B 107, 014508 (2023).
[22] S. Di Cataldo and L. Boeri, Metal borohydrides as ambient-pressure high-T_c superconductors, Phys. Rev. B 107, L060501 (2023).
[23] N. Dasenbrock-Gammon et al., Evidence of Near-Ambient Superconductivity in a N-Doped Lutetium Hydride, Nature 615, 244 (2023).
[24] P. Shan, N. Wang, X. Zheng, Q. Qiu, Y. Peng, and J. Cheng, Pressure-Induced Color Change in the Lutetium Dihydride LuH_2, Chin Phys Lett (2023).

[25] X. Ming, Y.-J. Zhang, X. Zhu, Q. Li, C. He, Y. Liu, B. Zheng, H. Yang, and H.-H. Wen, Absence of Near-Ambient Superconductivity in $LuH_{2\pm x}N_y$, arXiv:2303.08759 (2023).
[26] P. E. Blöchl, Projector Augmented-Wave Method, Phys Rev B 50, 17953 (1994).
[27] G. Kresse and J. Furthmüller, Efficiency of Ab-Initio Total Energy Calculations for Metals and Semiconductors Using a Plane-Wave Basis Set, Comput Mater Sci 6, 15 (1996).
[28] G. Kresse and J. Furthmüller, Efficient Iterative Schemes for *Ab Initio* Total-Energy Calculations Using a Plane-Wave Basis Set, Phys Rev B 54, 11169 (1996).
[29] J. P. Perdew, K. Burke, and M. Ernzerhof, Generalized Gradient Approximation Made Simple, Phys Rev Lett 77, 3865 (1996).
[30] A. Togo and I. Tanaka, First Principles Phonon Calculations in Materials Science, Scr Mater 108, 1 (2015).
[31] Y. Sun, F. Zhang, C.-Z. Wang, K.-M. Ho, I. I. Mazin, and V. Antropov, Electron-Phonon Coupling Strength from *Ab Initio* Frozen-Phonon Approach, Phys Rev Mater 6, 074801 (2022).
[32] G. L. Olcese, Interconfiguration Fluctuation of Cerium in CeN as a Function of Temperature and Pressure, J Physics F: Metal Physics 9, 569 (1979).
[33] A. Pebler and W. E. Wallace, Crystal Structures of Some Lanthanide Hydrides, J Phys Chem 66, 148 (1962).
[34] M. Mansmann and W. E. Wallace, The Structure of HoD_3, Journal de Physique 25, 454 (1964).
[35] A. Jain et al., Commentary: The Materials Project: A Materials Genome Approach to Accelerating Materials Innovation, APL Mater 1, 011002 (2013).
[36] S. Kirklin, J. E. Saal, B. Meredig, A. Thompson, J. W. Doak, M. Aykol, S. Rühl, and C. Wolverton, The Open Quantum Materials Database (OQMD): Assessing the Accuracy of DFT Formation Energies, npj Comput Mater 1, 15010 (2015).

Supplemental Material

Phase	Space group	Lattice parameter	Wyckoff site	Atoms	x	y	z
$Lu_8H_{21}N$	$P\bar{4}m2$	a= 7.1778 Å b= 7.1778 Å c= 5.1951 Å $\alpha = 90°$ $\beta = 90°$ $\gamma = 90°$	4k	Lu1	0.251	0.500	0.757
			4j	Lu2	0.737	0.000	0.730
			4j	H1	0.683	0.000	0.317
			4h	H2	0.240	0.240	0.000
			4i	H3	0.749	0.749	0.500
			1c	H4	0.500	0.500	0.500
			2g	H5	0.000	0.500	0.009
			4k	H6	0.838	0.500	0.343
			1d	H7	0.000	0.000	0.500
			1a	H8	0.000	0.000	0.000
			1b	N1	0.500	0.500	0.000

TABLE I. Crystallographic data of fully relaxed $Lu_8H_{21}N$ at 0 GPa.